JOURNAL OF PROPULSION AND POWER
Vol. 19, No. 2, March–April 2003

Numerical Simulation of Aerodynamic Damping for Flutter Analysis of Turbomachinery Blade Rows

R. Srivastava,* M. A. Bakhle,† and T. G. Keith Jr.‡
University of Toledo, Toledo, Ohio 43606

This paper describes the calculation of aerodynamic damping for prediction of flutter characteristics of turbomachinery blade rows. The unsteady aerodynamic blade loads are obtained by solving the Navier–Stokes equations on a dynamically deforming, body-fitted grid. Phase-lagged boundary conditions are used to model the nonzero interblade phase angle oscillations, and the energy exchange method is used to calculate the aerodynamic damping. The analysis is applied to calculate flutter of a transonic forward-swept fan configuration, which showed flutter at part speed conditions in wind-tunnel tests. The analysis successfully identified the most critical mode and the flow characteristics responsible for the observed flutter. The location of shock wave and variation of its strength were found to strongly influence the aerodynamic damping, with outboard stations providing the main contribution. The results also demonstrate that changes in blade shape impact the calculated aerodynamic damping, indicating the importance of using an accurate blade operating shape under centrifugal and steady aerodynamic loading. Sensitivity of the calculated aerodynamic damping to variation in inlet and exit conditions, the computational time steps, and blade natural frequency are also reported.

Introduction

NOISE reduction has become a significant aim in the design of modern turbomachinery fans. Aggressive blade designs with forward sweep and lean are being used to improve the noise characteristics. These geometric features coupled with the presence of shock waves can lead to flutter instability. Flutter problems, usually detected during the design phase, result in program delays and cost overruns, adversely impacting the development and maintenance costs. Numerical flutter prediction methods will help in achieving the design objectives and developing a flutter-free design.

Several methods have been developed for the prediction of aeroelastic characteristics of turbomachines with various degrees of fidelity. Aeroelastic analyses based on the energy exchange between vibrating blades and the surrounding fluid have been reported for turbomachines using semi-analytical methods,[1,2] linearized Euler method,[3] Euler methods,[4–6] linearized viscous method,[7] and viscous methods.[8–10] A limited number of coupled aeroelastic analyses of turbomachine configurations have also been reported.[11–13] Williams et al.[11] used a linear panel method to solve the eigenvalue problem. Gerolymos[12] and Srivastava and Reddy[13] solved the coupled aeroelastic equations based on an inviscid aerodynamic analysis.

Modern fans being designed to reduce noise are swept forward, have thin blade cross sections, and lean in the plane of rotation. These features coupled with transonic flow result in aeroelastic problems, requiring a three-dimensional viscous analysis to calculate accurately the flutter characteristics. For turbomachinery blade rows flutter is observed primarily in a single natural mode and is driven by either the presence of oscillating shock waves or stalled flow on the blade surfaces. Single-mode flutter can be captured using the energy-exchange method, which calculates the flow of energy between the vibrating blade and the surrounding fluid. An energy exchange method based on three-dimensional viscous unsteady aerodynamic code, reported in Ref. 6, is used in the present study. The objectives of the present study are 1) to calculate the aerodynamic damping for a forward-swept transonic fan, 2) to investigate its stability characteristics, and 3) to describe the flow features that result in instability.

Modern fan blades, by virtue of having a small thickness ratio coupled with forward sweep, can be highly flexible in the tip region. High rotational speed and large aerodynamic loading result in significant changes in blade shape. It is important to account accurately for these changes in the analysis. To investigate the sensitivity of damping calculations to changes in steady blade deflection, calculations are performed by changing the blade twist distribution. Also, results are obtained to investigate the effect of inlet and exit conditions and time step used in the analysis and sensitivity to variation of natural frequency. These studies are carried out to gain an understanding of issues that need to be addressed in flutter analyses of similar fan configurations.

Aerodynamic Analysis

The unsteady three-dimensional Navier–Stokes equations are solved for the internal flows of axial-flow turbomachinery components by use of a computer code entitled TURBO.[14,15] The solver can model multiple blade rows undergoing harmonic oscillations with arbitrary interblade phase angles (IBPAs). Good comparisons with experimental data for steady and unsteady aerodynamic analyses have been reported using the TURBO code.[16,17] A brief description of the solution method is provided here.

The Navier–Stokes equation in conservation form can be written as

$$\frac{\partial q}{\partial t} + \frac{\partial (E - E_v)}{\partial x} + \frac{\partial (F - F_v)}{\partial y} + \frac{\partial (G - G_v)}{\partial z} = 0 \qquad (1)$$

Here q is the vector of unknown flow variables in conservation form:

$$q = \begin{Bmatrix} \rho \\ \rho u \\ \rho v \\ \rho w \\ e \end{Bmatrix}$$

Received 29 March 2002; revision received 25 November 2002; accepted for publication 27 November 2002.

*Senior Research Associate, Department of Mechanical, Industrial and Manufacturing Engineering. Member AIAA.
†Senior Research Associate, Department of Mechanical, Industrial and Manufacturing Engineering.
‡Distinguished University Professor, Department of Mechanical, Industrial and Manufacturing Engineering. Associate Fellow AIAA.

with

$$E = \begin{Bmatrix} \rho u \\ \rho u^2 + p \\ \rho uv \\ \rho uw \\ u(e+p) \end{Bmatrix}, \qquad F = \begin{Bmatrix} \rho v \\ \rho uv \\ \rho v^2 + p \\ \rho vw \\ v(e+p) \end{Bmatrix}, \qquad G = \begin{Bmatrix} \rho w \\ \rho uw \\ \rho wv \\ \rho w^2 + p \\ w(e+p) \end{Bmatrix}$$

$$E_v = \begin{Bmatrix} 0 \\ \tau_{xx} \\ \tau_{xy} \\ \tau_{xz} \\ Q_x \end{Bmatrix}, \qquad F_v = \begin{Bmatrix} 0 \\ \tau_{yx} \\ \tau_{yy} \\ \tau_{yz} \\ Qy \end{Bmatrix}, \qquad G_v = \begin{Bmatrix} 0 \\ \tau_{zx} \\ \tau_{zy} \\ \tau_{zz} \\ Q_z \end{Bmatrix}$$

and

$$Q_x = u\tau_{xx} + v\tau_{xy} + w\tau_{xz} - \hat{q}_x$$

$$Q_y = u\tau_{yx} + v\tau_{yy} + w\tau_{yz} - \hat{q}_y$$

$$Q_z = u\tau_{zx} + v\tau_{zy} + w\tau_{zz} - \hat{q}_z$$

where ρ is the fluid density; u, v, and w are the Cartesian velocity components; e is the total internal energy per unit volume; and x, y, z are the Cartesian coordinates. Variables E, F, and G are the inviscid flux vectors; E_v, F_v, G_v are the viscous flux vectors, $\hat{q}_x$, $\hat{q}_y$, $\hat{q}_z$ are heat fluxes; and τ_{xx}, τ_{xy}, τ_{zy}, etc. are the stress vectors. A modified two-equation k–ε turbulence model is used for closure.[18]

The Navier–Stokes equation in Eq. (1) are transformed and recast in a generalized body-fitted coordinate system to simplify treatments of arbitrary geometries. The transformed equations are solved using an implicit finite volume upwind scheme. Flux vector splitting is used to evaluate the flux Jacobians on the left-hand side. The right-hand side fluxes are discretized using a high-order total-variation-diminishing(TVD) scheme based on Roe's flux difference splitting. Newton subiterations are used at each time step to find an approximate solution to the nonlinear finite volume discretization. Symmetric Gauss–Seidel relaxations are applied to solve the resulting linear system.

Aerodynamic Damping Calculation

Aerodynamic damping is obtained by calculating energy exchange between the vibrating blade and the surrounding fluid. The aerodynamic work on the blade is calculated by first obtaining the "steady" aerodynamic solution for a given operating condition. The blades are then forced into a prescribed harmonic motion (specified mode, frequency, and IBPA) in order to calculate the unsteady aerodynamic response and work per cycle of oscillation. The blade motion is simulated using a dynamic grid deformation technique. For harmonic motion in a selected normal mode, the displacement of any point on the blade $\boldsymbol{X}(x, y, z, t)$ can be written in terms of the generalized coordinate $q(t)$ and the modal deflection $\boldsymbol{\delta}(x, y, z)$ as

$$\boldsymbol{X}(x, y, z, t) = q(t)\boldsymbol{\delta}(x, y, z) \tag{2}$$

the work per cycle can then be calculated as

$$W = \oint\!\!\int_{\text{surface}} -p \cdot \mathrm{d}\boldsymbol{A} \cdot \left(\frac{\partial \boldsymbol{X}}{\partial t}\right) \mathrm{d}t \tag{3}$$

where p is the blade surface pressure and $\boldsymbol{A}$ is the surface area vector. For a harmonic motion prescribed as

$$q(t) = q_0 \sin(\omega t + \phi) \tag{4}$$

with amplitude of motion q_0, vibration frequency ω, and IBPA ϕ, the work per cycle of oscillation, using Eqs. (2–4), can be rewritten as

$$W = \oint\!\!\int_{\text{surface}} -p \cdot \mathrm{d}\boldsymbol{A} \cdot \boldsymbol{\delta} q_0 \omega \cos(\omega t + \phi)\, \mathrm{d}t \tag{5}$$

The aerodynamic damping associated with the blade motion is calculated by taking the ratio of work and the associated kinetic energy of the blade over one cycle of oscillation[19]

$$W/K_E = -8\pi\gamma \Big/ \sqrt{1-\gamma^2} \tag{6}$$

The damping ratio γ and the average kinetic energy K_E over one cycle of oscillation of the blade are defined as

$$\gamma = \frac{C}{C_{\text{cr}}} \tag{7}$$

$$C_{\text{cr}} = 2m\omega \tag{8}$$

$$K_E = \frac{1}{T} \oint \frac{1}{2} m V^2 \, \mathrm{d}t \tag{9}$$

where C is the damping, C_{cr} is the critical damping, m is the mass of the blade, V is the surface velocity caused by blade vibration, and T is the time period.

For small values of γ,

$$\sqrt{1-\gamma^2} \approx 1 \tag{10}$$

Combining Eqs. (10) and (6), the damping ratio can be calculated as

$$\gamma = -(W/8\pi K_E) \tag{11}$$

Negative aerodynamic damping implies flutter instability. Phase-lagged boundary conditions are used to calculate the nonzero IBPA oscillations, which eliminate the need to model multiple blade passages.

Results and Discussion

A 22-in. scale model of an experimental transonic fan with 22 blades (Fig. 1) was tested in a rig. The design operating condition for the model tested was mass flow of 44.85 kg/s with a relative tip Mach number of 1.4. The fan fluttered at part speed in the first natural mode[20] between the operating line and predicted stall line. The first mode shape of the blade (natural frequency 351 Hz) at

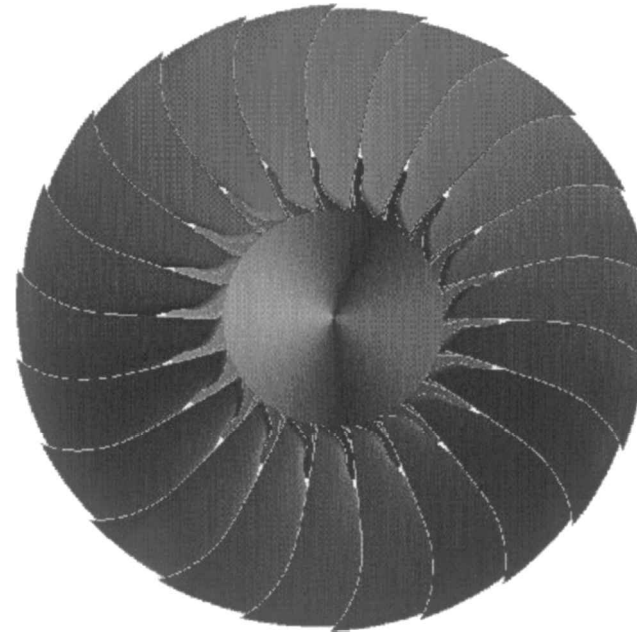

Fig. 1 Transonic fan.

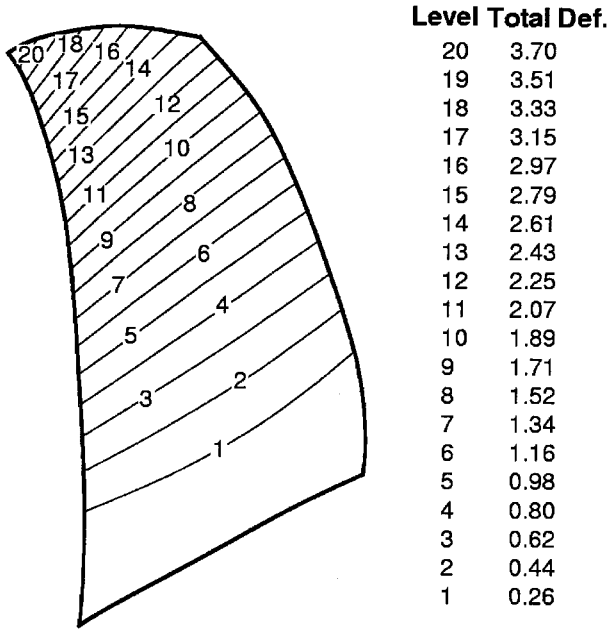

Fig. 2 First natural mode.

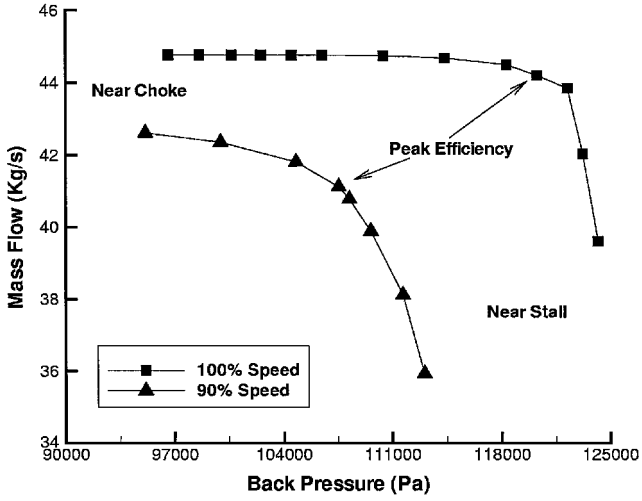

Fig. 3 Mass flow variation with back pressure.

design operating speed is shown in Fig. 2. The contours represent total displacement. The mode shows a high degree of twist bend coupling in the outboard region.

The aeroelastic analysis is carried out using a grid with 121 grid points in the axial direction, 39 grid points in the tangential direction, and 51 grid points in the spanwise direction. The results are presented for 90 and 100% rotational speed. The blade shape and modal properties for the design operating condition are used in the calculations presented here.

The variation of mass flow with backpressure for the fan at the two speed lines is shown in Fig. 3. The choke flow is captured by the analysis for both speeds. The highest backpressure at which a steady flow could be calculated was 113,050 Pa for 90% speed and 122,400 Pa for the 100% speed. Increasing the backpressure any further resulted in stalled flow with large separation on the suction surface in the midsection of the blade. This separation was found to be shock wave induced and prevented a steady mean flow from which the unsteady analysis could be carried out. During testing, for the 100% speed the predicted stall line was reached, whereas for the 90% speed stall was observed before the predicted stall line.[20] Comparison of fan performance at several speeds has been reported in Ref.[21]

Figure 4 shows the steady aerodynamic loading on the blade surfaces for 90% speed at a condition near the operating line. Shock-wave structures are evident from these figures. An oblique shock wave appears near the leading edge on the suction surface over the entire span. A normal shock wave extends across the blade passage in the aft section of the blade on the suction surface. For the inboard sections this shock wave is outside the blade passage (in front of blade leading edge) on the pressure surface side. However, the shock wave is completely ingested within the passage in the outboard sections of the blade. This shock-wave pattern is typical of a flow condition referred to as moderate-to-high loading on blades with a supersonic leading edge operating in subsonic axial flow. As the backpressure is increased, thus moving the operation point towards the stall line, the shock waves become stronger resulting in flow separation on the suction surface in the middle section of the blade. The separation is large enough to stall the blade, resulting in a breakdown of the numerical analysis. The observed breakdown of the analysis caused by flow separation could not be verified, as velocity profiles in the blade passage were not measured during the experiment.

Aerodynamic Damping Calculations

Experiments showed blade flutter at part speeds in the first natural mode for 32.73 IBPA (2 nodal diameter forward traveling wave).[20]

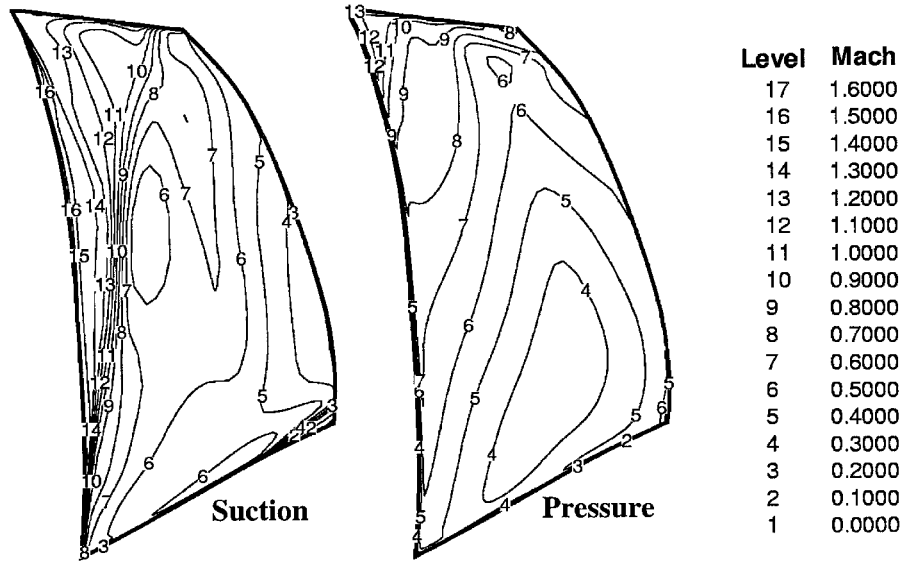

Fig. 4 Steady blade surface pressure near stall for 90 percent speed.

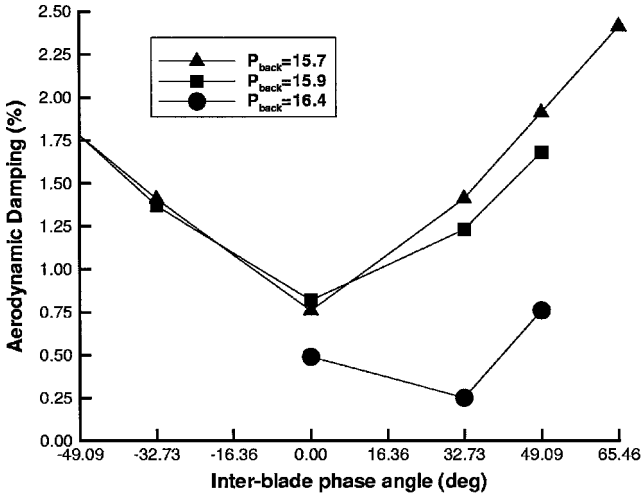

Fig. 5 Variation of aerodynamic damping with back pressure and IBPA for 90 percent speed.

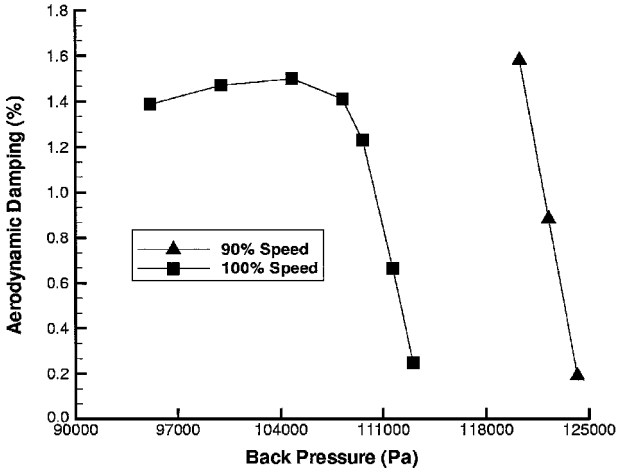

Fig. 6 Variation of aerodynamic damping with back pressure. Forced vibration in the first natural mode at 351 Hz and 32.73 deg IBPA.

To establish the most critical mode, the analysis was carried out for several pressure ratios and IBPAs. Figure 5 shows the aerodynamic damping calculated for several different back pressures and IBPAs for the 90% speed. For lower backpressures the least-stable IBPA was found to be 0 deg. However, as the backpressure was raised moving the fan operating condition towards the stall line the 32.73-deg IBPA (2 nodal diameter forward traveling wave) became least stable. This indicates that the analysis accurately calculated the 32.73-deg IBPA for the first natural mode to be the most critical for this geometry. Further analysis, therefore, was performed at 32.73-deg IBPA in order to identify the characteristics of the flow features impacting the stability.

The variation of aerodynamic damping with backpressure is shown in Fig. 6 at 32.73-deg IBPA for the two speed lines being analyzed. As the backpressure is increased from peak efficiency, the aerodynamic damping decreases rapidly, dropping to approximately 0.2% of critical damping at a backpressure of 113,050 Pa for 90% speed and 122,400 Pa for 100% speed.

Figure 6 also shows that the characteristics of variation of aerodynamic damping change significantly as the backpressure is varied. Increasing the backpressure beyond the peak efficiency results in a dramatic change in aerodynamic damping variation, and a rapid decrease is observed with increase in back pressure. To understand these variations, flow details were investigated for the 90% speed at backpressure values of 104,770, 109,600, and 113,050 Pa.

Figure 7 shows the distribution of work on the blade surface. Majority of the blade has little contribution towards establishing the flutter characteristics. Further, it can be seen that positive work is done over certain parts of the blade indicating a destabilizing contribution. These plots, when superimposed with relative Mach number plots, indicate that the positive work regions are centered around the shock-wave location. Also, it can be seen that the outboard sections of the blade contribute most significantly. This would suggest that resolving the details of the flowfield on the inboard sections might not be important for damping calculations. Hence, coarser grids can be used in the inboard sections, concentrating more grids in the outboard sections of the blade.

To investigate further, a pressure coefficient on suction surface at 90% span is plotted for the three backpressures in Fig. 8. Instantaneous pressure coefficient at five instants of time over one period of oscillation is shown. Steady pressure coefficient is also shown to highlight the variation of shock-wave location and its strength. As the backpressure is increased, the shock-wave moves upstream, and the variation in pressure over one cycle of blade

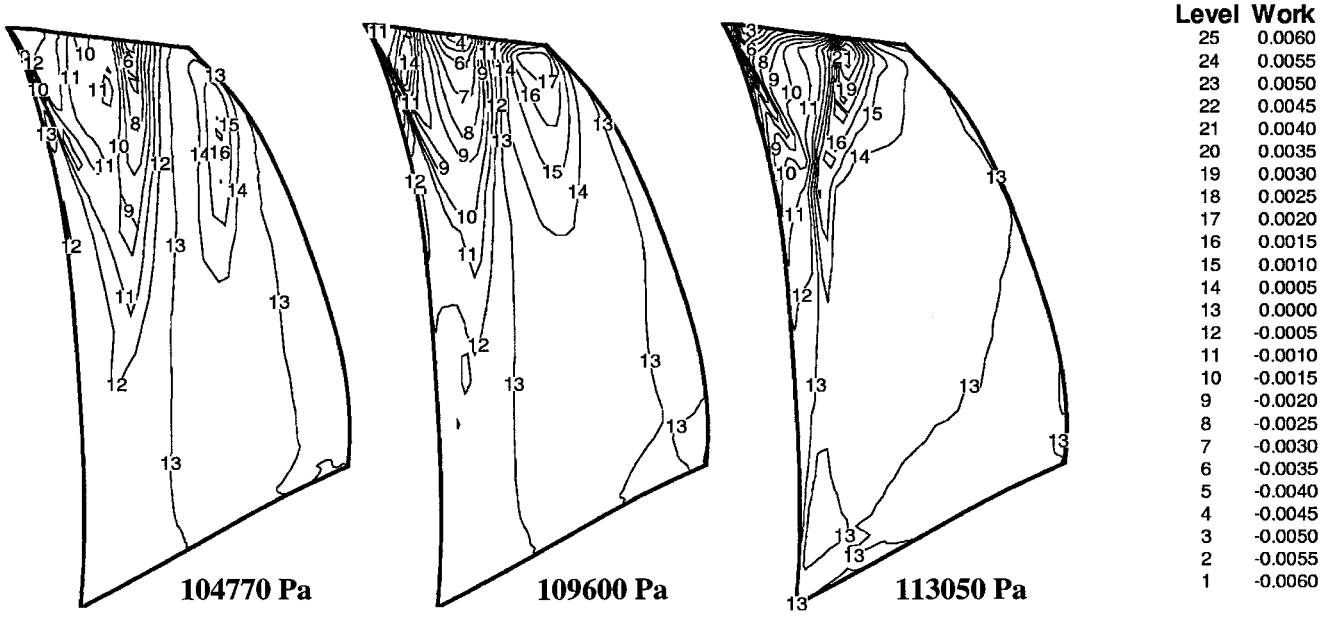

Fig. 7 Work distribution on blade surface for three back pressures at 90 percent speed.

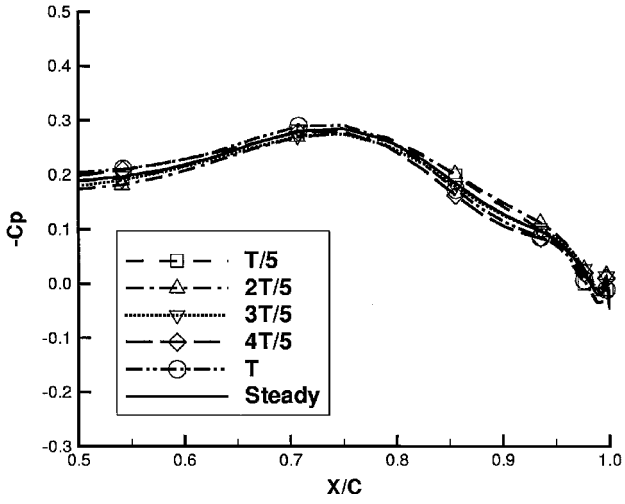

a) Backpressure 104770 Pa

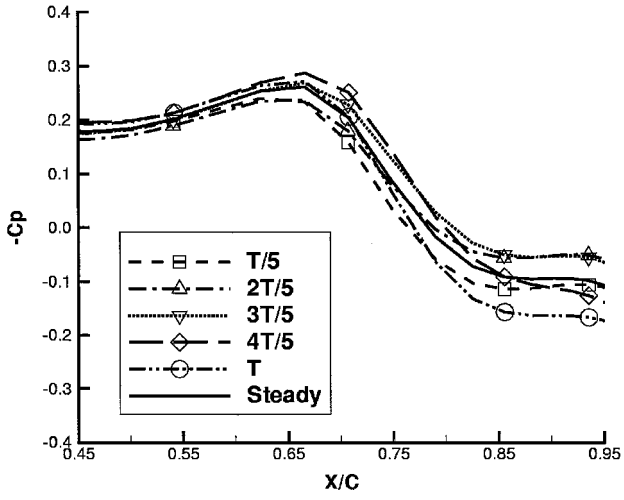

b) Backpressure 109600 Pa

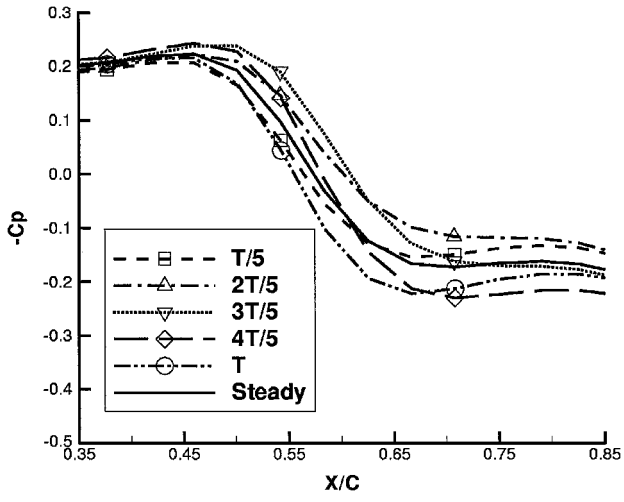

c) Backpressure 113050 Pa

Fig. 8 Pressure coefficient variation over one period of oscillation cycle for back pressures of 104770 Pa, 109600 Pa, 113050 Pa, 90 percent speed.

oscillation becomes larger. Also, a change in phase of pressure variation with blade motion can be seen with increase of backpressure. It is these changes that contribute towards increased positive work on the blade. Figures 6–8 together indicate that the location of shock wave and associated changes in strength and phase are the reasons for changes in characteristics of the variation of damping and are responsible for the observed flutter.

Analysis was also performed at the second natural vibration mode, which was stable in the experiment. The aerodynamic damping calculated was much higher than those for the first mode, indicating first mode to be the critical mode for flutter.

The blade natural vibration frequency for a rotor is proportional to the rotational speed. Therefore, for 90% speed the blade natural frequency would be lower than that at 100% speed. Because the calculations have been performed using blade properties for 100% geometry, the impact of change in frequency was investigated. Calculations for 90% speed and 32.73-deg IBPA were performed using natural frequency 20% higher and 20% lower than the design point natural frequency. These changes in frequency resulted in changes of less than 0.1% of critical damping ratio for the least-stable backpressure, indicating a low sensitivity to natural frequency for this geometry. Changes in rotational speed can also impact the mode shape; however, in the present study no attempt was made to alter the mode shape.

The numerical analyses in the present study were performed by prescribing experimentally measured total pressure, total temperature, radial and tangential flow angle at the inlet boundary, and measured static pressure profile at the exit boundary. However, during the design phase of a turbomachinery measured inlet and exit conditions are not available. Therefore, the impact of variation in inlet and exit conditions on the calculation of aerodynamic damping was investigated next. The analysis was carried out by using 1) uniform inflow and measured exit static-pressure profile, 2) measured inlet profile and exit static pressure calculated using radial equilibrium,[22] and 3) uniform inflow and exit static pressure calculated using radial equilibrium at an operating point along the 85% speed line. The effect of the boundary conditions on performance is shown in Fig. 9 and on aerodynamic damping in Fig. 10. The effect of using different boundary conditions at the inlet and exit is seen to be small for both performance and aerodynamic damping.

For the backpressure of 113,050 Pa at 90% speed, the experiment showed flutter, whereas the analysis predicted the fan to be marginally stable. Although the analysis correctly predicted the most critical mode, it did not predict a negative aerodynamic damping. A possible reason for that could be the use of an inaccurate operating blade shape. The analysis at the 90% speed was performed using the design speed geometry and characteristics. Generating the accurate operating blade shape for 90% speed requires iterating between steady aerodynamic analysis and structural analysis an expensive calculation. Therefore, to investigate the effects of changes in blade shape under operating condition the analysis was carried out on a deformed blade shape obtained by altering the twist distribution along blade span. The blade twist was changed from midspan to tip varying linearly from zero change at midspan to 0.5-deg change at the tip. The change in twist distribution was such that it increased the

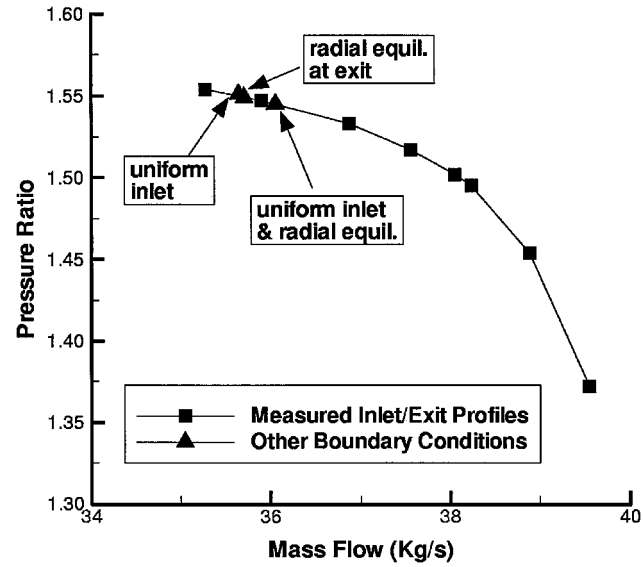

Fig. 9 Effect of inlet and exit boundary conditions on the performance at 85 percent speed operating line.

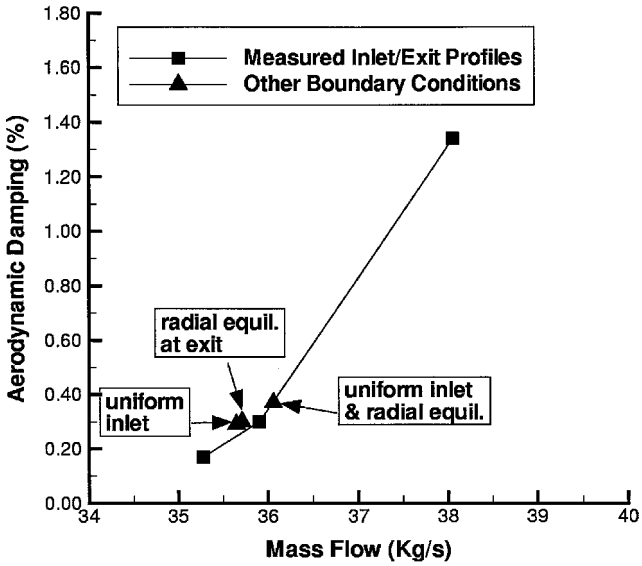

Fig. 10 Effect of inlet and exit boundary conditions on the aerodynamic damping at 85 percent speed operating line.

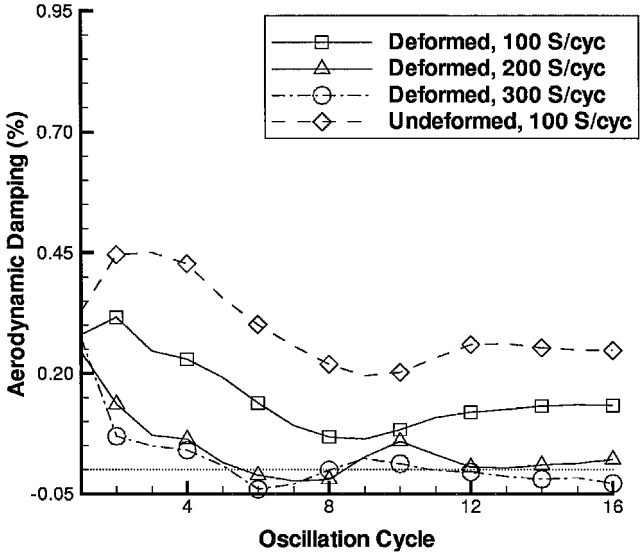

Fig. 11 Effect of time steps and change in twist distribution for a 0.5 deg change in twist at tip of the blade at 90 percent speed and 113050 Pa.

incidence of the blade. Structural analysis showed the blade twist change because of changes in centrifugal and aerodynamic loading at the tip to be of this order for the 90% speed. The variation in aerodynamic damping with oscillation cycles for the deformed geometry is shown in Fig. 11. The changes in twist reduce the damping moving it closer to instability.

Earlier studies had shown that smaller time steps have moderate impact on the damping calculations. As the calculated damping is close to zero, the impact of smaller time steps was also investigated for the deformed geometry at this flow condition. Most of the analysis was performed using 100 steps per oscillation cycle in order to minimize the computational cost. The computational cost varies linearly with number of steps per cycle used in the analysis. Three different time steps were used: 100, 200, and 300 steps per oscillation cycle. The impact of time-step size is also shown in Fig. 11. A measurable change in calculated aerodynamic damping is seen with smaller time-step size moving the results closer to the flutter boundary. Therefore, for more accurate aerodynamic damping smaller time steps and an accurate blade shape under operating conditions should be used. However, for investigating trends larger time steps and design point blade geometry are adequate.

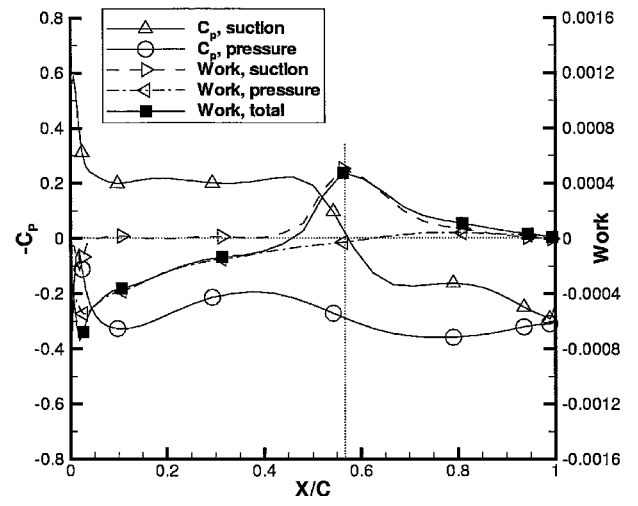

a) Original geometry

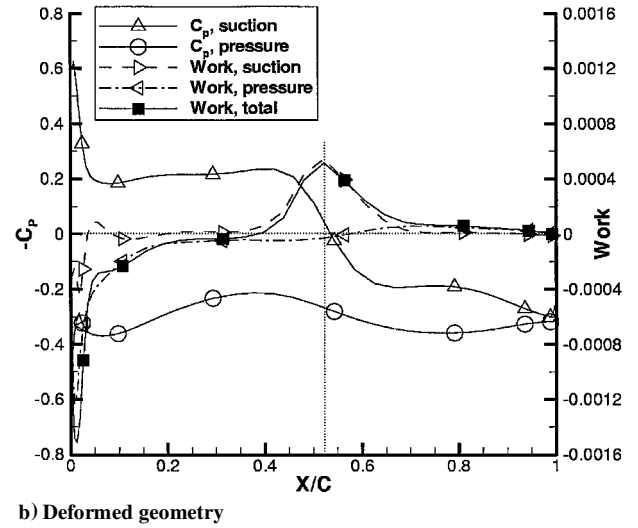

b) Deformed geometry

Fig. 12 Pressure coefficient and work distribution at 95 percent span for 90 percent speed and 113050 Pa.

Figure 12 compares the steady pressure coefficient and work contributions from the suction and pressure surfaces at the 95% span location for both deformed and undeformed blade geometries. The results for the original geometry are shown in Fig. 12a and for the deformed geometry in Fig. 12b. These comparisons were made to understand the differences in calculated damping for the deformed shape better. As seen, the suction surface contributes to positive work, whereas the pressure surface contributes to negative work providing a stabilizing influence. However, there are two main differences that are observed from these figures. First, we find that for the deformed geometry the shock wave on the suction surface has moved upstream by roughly 5% of chord length, along with the work contribution associated with this shock wave. Only minor changes in the level of work are observed. A second change, which is more significant from the work perspective, is seen on the pressure surface. The area of negative work in the leading-edge region is reduced, and the peak is higher but narrower for the deformed shape. This change contributes to the reduction in the damping for the deformed shape.

Primary reason for the difference in damping was found to be the motion of shock-wave on pressure surface. Figure 13 shows the steady pressure contours, and Fig. 14 shows the instantaneous pressure contours at five instants of time over the oscillation cycle for original and deformed geometry at 95% span. The steady contours show that a normal shock-wave extends from the suction surface across the blade passage. For the original geometry the shock wave intersects the pressure surface at the leading-edge, whereas for the deformed geometry the shock-wave is just ahead of the leading-edge.

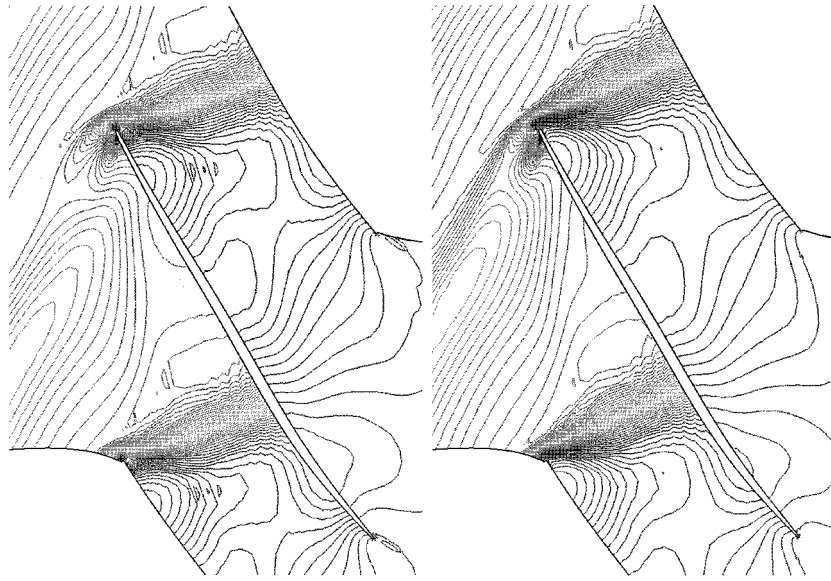

Original geometry **Deformed geometry**

Fig. 13 Steady pressure contours at 95 percent span for 90 percent speed and 113050 Pa.

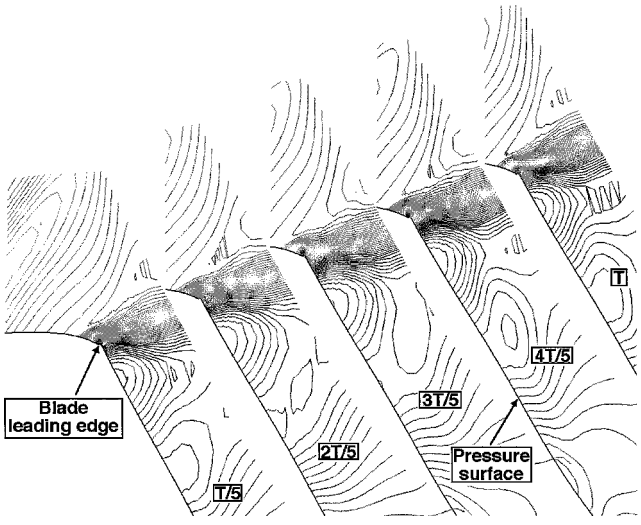

a) Original geometry

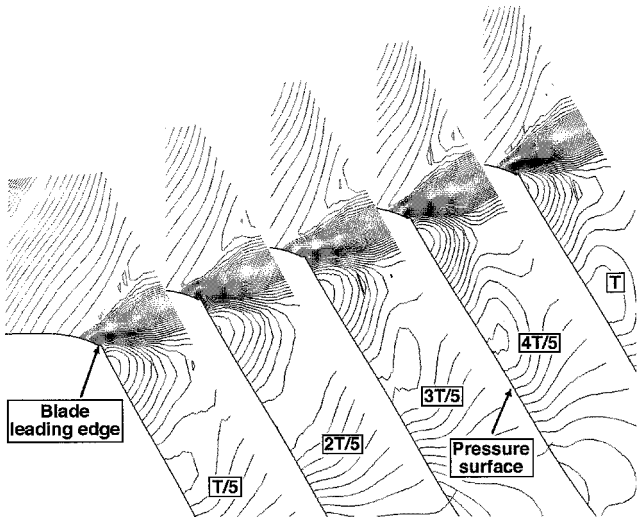

b) Deformed geometry

Fig. 14 Instantaneous pressure contours at five instants of time, over one cycle of oscillation with period T. Near pressure surface leading edge at 95 percent span for 90 percent speed and 113050 Pa.

Figure 14 shows the shock-wave movement over one oscillation cycle for deformed and undeformed geometries. Instantaneous pressure contours near the pressure surface leading edge are shown for five time instants over one cycle of oscillation. For ease of comparison, these contours are plotted next to each other going from left to right with increasing time. The pressure surface, leading edge, and time instants corresponding to the contour are marked on the figures. From Fig. 14a it is seen that the shock wave stays on the blade surface over the oscillation cycle for the original geometry. Whereas, for the deformed geometry (Fig. 14b) the shock wave intersects the blade for part of the oscillation cycle, moving on and off the blade surface over the oscillation cycle. This shock-wave motion on and off the blade surface is the reason for differences in work contribution on the pressure surface between the two geometries. The effect of this motion is to reduce the overall stabilizing effect from the pressure surface reducing the aerodynamic damping for the deformed geometry.

Computational Cost

A typical analysis required roughly 1000 steps for a steady solution and 16 oscillation cycles with 100 steps per cycle for the aerodynamic damping calculations. The analyses were carried out using the Cray C-90 computer of the National Aerospace Simulation computational facility at NASA Ames Research Center. Each analysis required roughly 95 M Words of computer memory and one hour of computational time per 100 steps.

Summary

An aeroelastic analysis program based on the Navier–Stokes equation has been used to calculate the aerodynamic damping for a forward-swept transonic fan geometry. Calculated variations of aerodynamic damping with backpressure and IBPA are presented for a condition where flutter occurred during testing. Although a negative aerodynamic damping was not calculated, the analysis yielded good results and trends. The analysis correctly calculated the most critical mode and IBPA of flutter. Also, the trend for calculated aerodynamic damping clearly indicated a negative aerodynamic damping would result with further increasing the backpressure. However, the analysis showed that stalled flowfield with large separation would emerge, causing the numerical analysis to break down for any further increase of the backpressure.

The location and strength of the shock-wave were found to be the main factor affecting the stability. Results showed the stabilizing and destabilizing effects were strongly influenced by the shock-wave

and were restricted to outboard stations of the blade. Detailed examination of the flow features indicated that the shock wave on suction surface had a destabilizing effect and resulted in a large destabilizing area of positive work centered around the shock wave. The area of the destabilizing effects depended on the location and strength of the shock wave. Higher backpressure moved the shock wave forward and also increased the area of positive work causing the destabilizing influence to increase.

Study was also performed to understand the effect of various parameters on the calculation of aerodynamic damping. The effect of inlet and exit boundary condition on aerodynamic damping calculation was found to be small. The effect of time steps and operating blade shapes were found to be moderate and of significance in the vicinity of flutter boundary. It was found that accurate blade shape under operating conditions and smaller time steps are needed to accurately predict the flutter boundary. However, away from the flutter boundary larger time steps and design point blade geometry can be used for calculating trends. The study also indicated that vibration frequency had relatively small impact on aerodynamic damping.

Acknowledgments

This work was performed under the contract NAS3-01116 from the Structural Mechanics and Dynamics Branch of NASA John H. Glenn Research Center, Cleveland, Ohio. The authors also wish to thank Josef Panovsky of Honeywell Engines, Systems, and Services, Phoenix, Arizona, for his valuable help and discussions.

References

[1]Lane, F., and Friedman, M., "Theoretical Investigation of Subsonic Oscillating Blade-Row Aerodynamics," NACA TN 4136, Feb. 1958.

[2]Smith, S. N., "Discrete Frequency Sound Generation in Axial Flow Turbomachines," British Aeronautical Research Council, R&M 3709, London, March 1972.

[3]Verdon, J. M., "Unsteady Aerodynamic Methods for Turbomachinery Aeroelastic and Aeroacoustic Applications," *AIAA Journal*, Vol. 31, No. 2, 1993, pp. 235–250.

[4]He, L., "An Euler Solution for Unsteady Flows Around Oscillating Blades," *Journal of Turbomachinery*, Vol. 112, No. 4, 1989, pp. 714–722.

[5]Gerolymos, G. A., and Vallet, I., "Validation of 3-D Euler Methods for Vibrating Cascade Aerodynamics," American Society of Mechanical Engineers, Paper 94-GT-294, June 1994.

[6]Bakhle, M. A., Srivastava, R., Keith, T. G., Jr., and Stefko, G. L., "A 3D Euler/Navier–Stokes Aeroelastic Code for Propulsion Applications," AIAA Paper 97-2749, July 1997.

[7]Clark, W. S., and Hall, K. C., "A Time-Linearized Navier–Stokes Analysis of Stall Flutter," *Journal of Turbomachinery*, Vol. 122, No. 3, 2000, pp. 467–476.

[8]Giles, M., and Haimes, R., "Validation of a Numerical Method for Unsteady Flow Calculations," American Society of Mechanical Engineers, Paper 91-GT-271, June 1991.

[9]Siden, L. D. G., "Numerical Simulation of Unsteady Viscous Compressible Flows Applied to a Blade Flutter Analysis," American Society of Mechanical Engineers, Paper 91-GT-203, June 1991.

[10]He, L., and Denton, J. D., "Three Dimensional Time Marching Inviscid and Viscous Solutions for Unsteady Flows Around Vibrating Blades," *Journal of Turbomachinery*, Vol. 116, No. 3, 1994, pp. 469–476.

[11]Williams, M. H., Cho, J., and Dalton, W. N., "Unsteady Aerodynamic Analysis of Ducted Fans," *Journal of Propulsion and Power*, Vol. 7, No. 5, 1991, pp. 800–804.

[12]Gerolymos, G. A., "Coupled 3-D Aeroelastic Stability Analysis of Bladed Disks," American Society of Mechanical Engineers, Paper 92-GT-171, June 1992.

[13]Srivastava, R., and Reddy, T. S. R., "Comparative Study of Coupled-Mode Flutter-Analysis Methods for Fan Configurations," *Journal of Propulsion and Power*, Vol. 15, No. 3, 1999, pp. 447–453.

[14]Janus, J. M., "Advanced 3-D CFD Algorithm for Turbomachinery," Ph.D. Dissertation, Dept. of Aerospace Engineering, Mississippi State Univ., Mississippi, May 1989.

[15]Chen, J. P., "Unsteady Three-Dimensional Thin-Layer Navier–Stokes Solutions for Turbomachinery in Transonic Flow," Ph.D. Dissertation, Dept. of Aerospace Engineering, Mississippi State Univ., Mississippi, Dec. 1991.

[16]Chen, J. P., and Barter, J., "Comparison of Time-Accurate Calculations for the Unsteady Interaction in Turbomachinery Stage," AIAA Paper 98-3292, July 1998.

[17]Barter, J. W., Vitt, P. H., and Chen, J. P., "Interaction Effects in a Transonic Turbine Stage," American Society of Mechanical Engineers, Paper 2000-GT-0376, May 2000.

[18]Shih, T.-H., Liou, W. W., Shabbir, A., Yang, Z., and Zhu, J., "A New k–ε Eddy Viscosity Model for High Reynolds Number Turbulent Flows," *International Journal of Computers and Fluids*, Vol. 24, No. 3, 1995, pp. 227–238.

[19]Carta, F. O., "Coupled Blade-Disk-Shroud Flutter Instabilities in Turbojet Engine Rotors," *Journal of Engineering for Power*, Vol. 89, No. 3, 1967, pp. 419–426.

[20]Fite, B. E., "Aerodynamic Overview of the NASA/Honeywell Quiet High Speed Fan Test," Noise Reduction/QAT Technical Working Group Meeting, Sponsored by NASA Langely Research Center, April 2001.

[21]Panovsky, J., Bakhle, M. A., and Srivastava, R., "Flutter Characteristics of a Forward-Swept Fan," *Proceedings of the 7th National Turbine High Cycle Fatigue Conference*, Published by Universal Technology Corp., Dayton, Ohio, April 2002.

[22]Horlock, J. H., *Axial Flow Turbines—Fluid Mechanics and Thermodynamics*, Krieger, Malabar, FL, 1982, pp. 148 and 1113.